Materials Advances

ROYAL SOCIETY OF CHEMISTRY

PAPER

View Article Online
View Journal | View Issue

Cite this: *Mater. Adv.*, 2022, 3, 7881

High performance NiO_x nanoplatelet based films by a scrape-coating method for bifunctional electrochromic and energy storage devices†

Xinyu Tao,[a] Yong Zhang, *[a] Jingyi Cai,[a] Hark Hoe Tan,[b] Jiewu Cui,[a] Yan Wang,[a] Xia Shu,[a] Zhenhong Dai, *[c] Yongqiang Qin,[a] Jiaqin Liu[de] and Yucheng Wu *[a]

Nickel oxide (NiO_x) is considered a promising candidate for constructing complementary electrochromic devices with tungsten oxide. However, the low electrochromic performance of NiO films has been a hindrance to its practical applications. In this study, crystal oriented NiO_x nanoplatelets with nickel vacancies were prepared using a facile chemical precipitation method and scrape-coated onto FTO substrates. The morphology and electrochromic properties of the obtained porous films can be controlled by adjusting the amount of polyethylene glycol in the slurry. The films exhibit an outstanding optical modulation range (63.09%), fast switching speed (1.7 s for colouring/1.5 s for bleaching) and high colouration efficiency (83.8 $cm^2\ C^{-1}$) using propylene carbonate/$LiClO_4$ as an electrolyte. The films also present superior cycling stability, maintaining 95% of the original optical modulation after 1000 cycles, as well as high colouring efficiency (45.12 $cm^2\ C^{-1}$) and good reversibility. The correlation between the Ni vacancy formation and crystal facets of the NiO_x was illuminated based on density functional theory (DFT) simulation. Furthermore, the electrochromic devices (ECDs) and flexible films of NiO_x were fabricated in addition, and electrochromic devices were prepared to demonstrate their electrochromic/energy storage bifunctionality and low temperature annealing properties, which can open up applications in wearable/energy storage devices and flexible displays. In addition, the ease and high efficiency of the scrape-coating technique makes it possible to commercially produce high performance electrochromic NiO_x nanoplatelet films.

Received 11th July 2022,
Accepted 8th August 2022

DOI: 10.1039/d2ma00816e

rsc.li/materials-advances

Introduction

Electrochromic (EC) materials have demonstrated their capability to harness solar energy in the visible and infrared regions owing to their advantages of steady reversible modulation in optical transmission/absorption/reflection driven by a low voltage.[1–4] In the past few years, electrochromic materials have exhibited great potential in energy saving and environmental friendliness which leads to a wide range of applications in areas such as smart windows for energy-efficient buildings, low-power displays, self-dimming rear-view mirrors for automobiles, and e-skins.[5–10] Inorganic EC materials have been extensively studied due to their excellent chemical properties and thermal stability. Among them, tungsten oxide (WO_3) as a stable cathodic EC material has been fully developed in the past few years.[11–14] As the most promising candidate for an anode EC material complementary to WO_3 in EC devices, nickel oxide (NiO) has received a lot of research interest due to high coloration efficiency, neutral coloured-state and cost effectiveness;[15–17] however, it suffers from low optical transmittance modulation, poor cycling stability and slow response speed.[18,19]

To circumvent these shortcomings, varies attempts have been made. Chiang *et al.*[20] prepared NiO nanocrystalline films using a thiourea-assisted method, and found that the optical transmittance modulation of the films increased from 10% to 60% in an aqueous KOH electrolyte as the grain size decreased, whilst the coloration efficiency increased from 12 to 25.2 $cm^2\ C^{-1}$. Zhang *et al.*[21] used a simple two-step solution method to

[a] *School of Materials Science and Engineering, Hefei University of Technology, Hefei, China. E-mail: zhangyong.mse@hfut.edu.cn, ycwu@hfut.edu.cn*
[b] *The Australian National University, Electronic Materials Engineering, Research School of Physics and Engineering, Canberra, Australia*
[c] *Department of Physics, Yantai University, Yantai, China. E-mail: zhdai@ytu.edu.cn*
[d] *Institute of Industry & Equipment Technology, Hefei University of Technology, Hefei, China*
[e] *Engineering Research Center of Advanced Composite Materials Design & Application of Anhui Province, Hefei University of Technology, Hefei, China*

† Electronic supplementary information (ESI) available. See DOI: https://doi.org/10.1039/d2ma00816e

synthesize graded SnO_2@NiO nanoflake array structures, and the prepared films had high contrast (85.3%) and fast switching speed (1.7 s for colouring/2.4 s for bleaching) in the KOH electrolyte. Basically, a high transmittance change can be obtained in alkaline electrolyte solutions for NiO; however, it is subjected to poor cycling stability which presents an exceptional challenge especially to complement WO_3 for device construction. In lithium ion electrolytes, NiO shows much better cycling stability feasible for producing electrochromic devices with WO_3, but its low transmittance change has hindered its practical applications.[22–25] Nandy *et al.*[26] reported that the low-dimensional nanostructured NiO has a great impact on the local current transport mechanism, and NiO can achieve better hole conductivity in an oxygen atmosphere due to the presence of Ni^{3+}, which in turn improves the film properties. In addition, the forked finger structure can significantly favor the device performance, nevertheless, the conventional planar mode was proposed in our work in the electrochromic device construction in order to maintain the uniformity of colour change.[27] Therefore, magnetron sputtering is an effective method to realize stable and reliable electrochromic performance of NiO_x films in Li^+ electrolytes.[28–30] For example, Qiu *et al.*[31] prepared NiO_x films by direct current magnetron sputtering which achieved up to 62% transmittance change in 1 M PC/$LiClO_4$, but their colouring and bleaching times were as long as 17 and 9.8 s, respectively. Acua *et al.*[32] adjusted the radio frequency power to vary the crystallinity and grain size of the NiO films, achieving 55% transmittance change in 1 M PC/$LiClO_4$, but the colouring and bleaching times were still 4.1 and 9.9 s, respectively. Guo *et al.*[33] prepared NiO_x thin films by reactive magnetron sputtering and showed pronounced discolouration behaviour of NiO_x in Li^+ electrolytes by implanting nickel vacancies in the films. Nevertheless, magnetron sputtering makes it difficult to manipulate the film architecture and dense films are usually obtained, which results in a slow switching speed.[34] Moreover, stringent equipment and high vacuum environment are required for magnetron sputtering which also makes it cost effective and enables large area production of NiO_x films.[35] Therefore, rational design of a NiO colour-tuning unit and suitable architecture is essential for the production of high performance NiO_xNiO_x EC films. Moreover, the development of high quality NiO films compatible with Li^+ electrolytes has obvious advantages in producing high performance electrochromic devices as well as visual energy storage devices for practical applications.[36–39]

In this work, we designed a scrape-coating method for producing high quality NiO_x nanoplatelet (NP) films with superior electrochromic performance as well as energy storage properties. The films were obtained by scraping and coating crystal oriented NiO_x NPs well-dispersed in an EC slurry using a microelectronic printer. The NiO_x NPs feature well-defined nickel vacancies prepared based on a facile but well-controlled chemical precipitation method. In addition, it was found that polyethylene glycol 4000 (PEG4000) plays a crucial role in determining the homogeneity of the NPs in the slurry as well as EC performance of the film which can be ascribed to a co-dispersing and bonding effect. The NiO_x NP films coated on the FTO substrate exhibited ultra-high contrast (ΔT = 63.09%), fast response (1.7 s for colouring/1.5 s for bleaching), high tinting efficiency (83.8 $cm^2\ C^{-1}$), good cycling stability (95% retention after 1000 cycles), and interesting energy storage performance, while the prepared devices demonstrate its electrochromic/energy storage bifunctional properties. The film coated on the PEN-ITO substrate suggested both superior EC performance and good mechanical flexibility of the NiO_x NP films. The correlation between the Ni vacancy formation and crystal facets of NiO was illuminated based on density functional theory (DFT) simulation. The enhancement mechanism of the NiO_x NPs and PEG4000 on the EC performance of the films was proposed. The ease and efficiency of scrape-coating and the ability to produce large-area films show its potential and advantages for commercialisation purposes.

Experimental

Fabrication of NiO_x nanoplatelets

NiO_x NPs were prepared based on a chemical precipitation method,[40] which was modified and improved in this work. 0.05 mol of nickel nitrate hexahydrate ($Ni(NO_3)_2{\cdot}6H_2O$, AR grade 98%) was added to beaker A containing 50 mL of anhydrous ethanol to form 1 mol L^{-1} ethanolic solution of $Ni(NO_3)_2$. 48 mL of a 1 mol L^{-1} aqueous solution of NaOH (AR grade 98%) was prepared in beaker B. Configure 48 mL of 1 mol L^{-1} aqueous NaOH (AR grade, 98%) solution in beaker B. The two solutions from beakers A and B were mixed and stirred slowly to obtain a light green $Ni(OH)_2$ suspension. The suspension was centrifuged and washed with deionised (DI) water and repeated three times to obtain a $Ni(OH)_2$ precipitate, with the speed of centrifugation being increased from 6000 to 8000 rev min^{-1} and 10 000 rev min^{-1} sequentially. The resulting $Ni(OH)_2$ precipitate was dried at 80 °C for 12–18 h and then ground in a mortar for 30 min to obtain a green powder. The powder was sintered at 270 °C for 2 h to obtain NiO_x NPs.

Fabrication of NiO_x electrochromic slurry

The NiO_x EC slurry was obtained by adding 250 mg of NiO_x powder to 5 mL of DI water for dispersion, followed by 5 mL of anhydrous ethanol and 0–0.50 g of PEG4000. The slurry was obtained after evaporating 85% of the solution by magnetic stirring for 70 °C at 300 rev min^{-1}.

Fabrication of NiO_x NP films

The high performance NiO_x NP films were fabricated on fluorine-doped tin oxide (FTO) conductive glass substrates using a facile scrape-coating method. The FTO substrates were first treated in acetone, ethanol, DI water and a UV cleaner in sequence before use. The film preparation and subsequent tests were kept under identical environmental conditions (temperature around 25 °C and humidity below 50%). The prepared NiO_x slurry was then applied to the FTO using a microelectronic printer (SCIENTFIC 3A, Prtronic, China) at a scraping speed of 6 mm s^{-1} at a distance of 20 μm from the FTO surface to obtain a coating of 20 μm thickness. The coated FTO substrates were

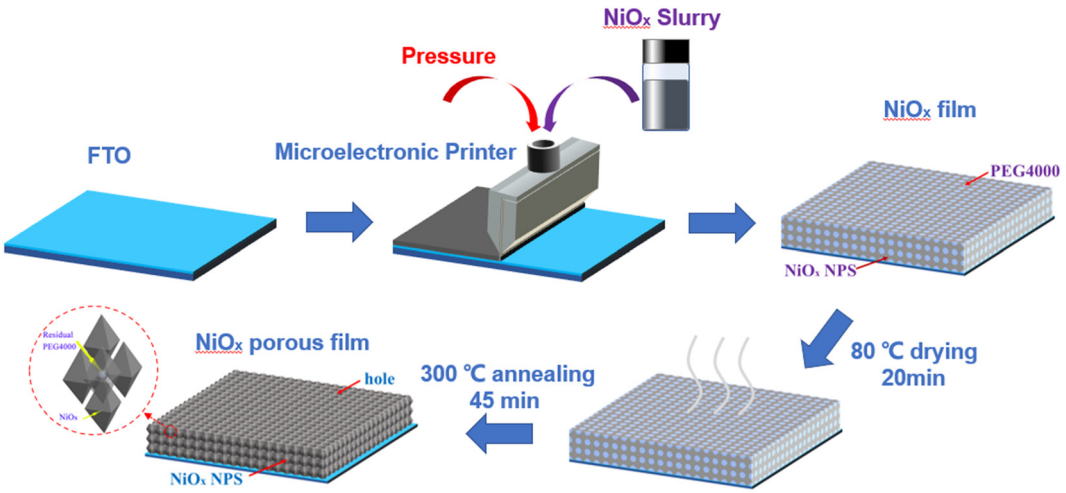

Fig. 1 Flow chart of NiO_x NP film preparation.

then dried at 80 °C for 20 min and before being annealed at 300 °C for 45 min to remove PEG4000 and other organic matter to obtain NiO_x NP porous films. A schematic of this process is illustrated in Fig. 1.

Characterization and measurements

Characterization of the morphological features and structures of NiO_x NP films and NiO_x NPs was carried out by field emission electron microscopy (FESEM, SU8230, Hitachi, Japan), X-ray diffractometry (XRD, X-Pert PRO MPD, Panaco, The Netherlands, Cu Kα radiation) and transmission electron microscopy (TEM, JEM-2100F, Nippon Electron, Japan). The elemental composition and valence of the film surface was analyzed by X-ray photoelectron spectroscopy (XPS, ESCALAB 250Xi, Thermo, USA). The residual organic matter in the films was detected by Fourier transform infrared spectrometry (FTIR, Nicolet IS50 iN10, Thermo Fisher, USA). Cyclic voltammetry (CV) and chronoamperometry (CA) were carried out in a three-electrode electrochemical workstation (CHI760E, Shanghai Chenhua, China) with 1 M PC/$LiClO_4$ as the electrolyte, with the NiO_x films coated on FTO (0.6 × 3 cm^2) as the working electrode, platinum wire and Ag/AgCl electrodes as counter and reference electrodes, respectively. CV was measured at room temperature (25 °C) at a scan rate of 50 mV s^{-1} over a range of −1.0 to 1.7 V. The transmittance spectra of the films were measured using a UV-VIS-NIR spectrophotometer (UV-3600, Shimadzu, Japan) in the

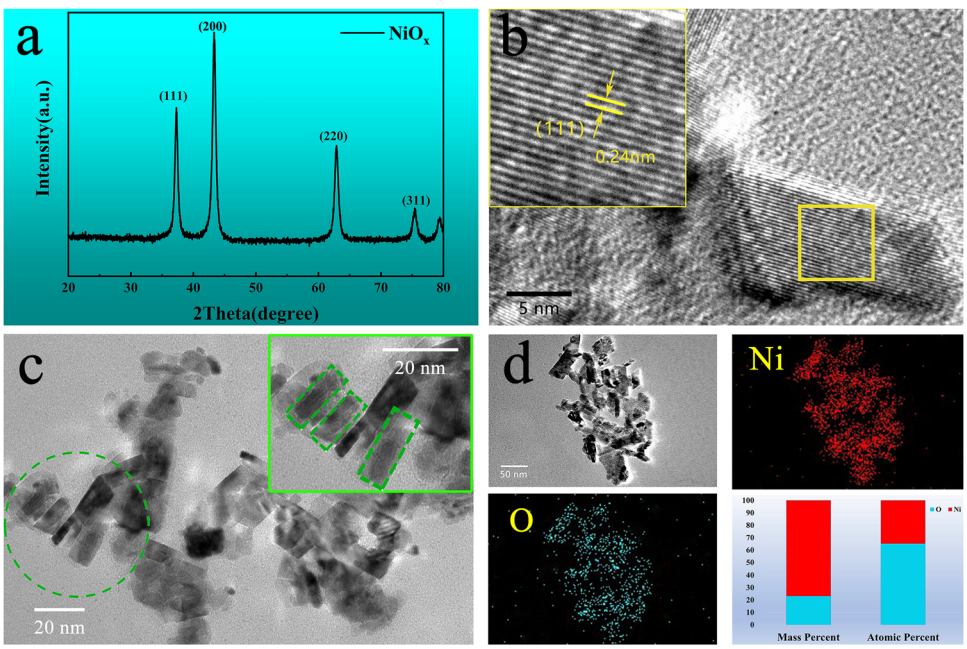

Fig. 2 Structural and chemical properties of NiO_x NPs. (a) XRD pattern; (b) high resolution TEM image; (c) TEM image; (d) Ni and O elemental map and their mass and atomic percentages.

wavelength range 380–760 nm in the fully faded (−1.0 V) and fully colored (1.7 V) states, as well as *in situ* optical transmittance at 550 nm with the same electrolyte of 1 M PC/$LiClO_4$.

Results and discussion

X-ray diffraction (XRD) was used to characterize the phase structure of the obtained NiO_x NPs as shown in Fig. 2(a). The diffraction pattern of the NPs was determined to be a bunsenite NiO structure in the cubic $Fm\bar{3}m$ space group (JCPDS 047-1049) with prominent characteristic diffraction peaks at 2θ values of 37.2°, 43.2° and 62.8°, which can be indexed to (111), (200) and (220) crystalline planes, respectively, indicating good crystallinity of the prepared NiO_x NPs. High resolution transmission electron microscopy (HRTEM) in Fig. 2(b) shows lattice fringes of a nanoplatelet-like NiO_x crystal exposing the plane with 0.24 nm spacing between lattice planes, corresponding to the (111) plane of cubic NiO indicating oriented growth of the NPs along the (111) plane.[41] Fig. 2(c) shows the grain size of the NiO_x nanoparticles, appearing with more of a nanoplatelet-like morphology with a plate thickness of approximately 12 nm along the [111] direction, which is essentially the same as the average particle size of NiO_x NPs calculated by the Debye–Scherrer formula from the XRD data. Fig. 2(d) shows the distribution of Ni and O elements in the NiO_x NPs, as well as the mass and atomic percentages of Ni and O where the NiO_x NPs appear to be oxygen rich. To investigate detailed surface chemistry information of the NPs, X-ray photoelectron spectroscopy (XPS) detailed spectra of the O 1s and Ni 2p of the NPs were obtained as shown in Fig. S2a and b (ESI†), respectively. For the O 1s spectrum, the peak at 529.2 eV to lattice oxygen ions in the NiO whilst the peak at 530.9 eV can be indexed to defective oxygen atoms near nickel vacancies where Ni^{3+} is generated.[42] The XPS spectrum of Ni 2p consists of two spin–orbit doublet characteristics of Ni^{3+} and Ni^{2+} and two spin–orbit shakeup satellites. The peaks at 873.8 and 855.8 eV are assigned to Ni^{3+}, while the peaks at 871.9 and 853.9 eV belong to Ni^{2+}.[43] Also, quantitative analysis by XPS determines a stoichiometric ratio of 1.47 for O to Ni (O : Ni = 1.47). The presence of Ni^{3+} has been proposed as the key factor generating a coloration effect and the capacity of the reversible intervalence charge transfer between the adjacent Ni^{2+} and Ni^{3+} reveals the EC performance of NiO_x in PC/$LiClO_4$.[44]

The NiO_x slurry was obtained by dispersing the NPs in the DI water and anhydrous ethanol by adding a certain amount of PEG4000. Uniform thin NiO_x NP films were fabricated by scraping and coating the slurry using a microelectronic printer. It was found that PEG4000 plays a crucial role in determining the film quality. Fig. 3(a) and Fig. S3a–c (ESI†) shows the surface morphology of the NiO_x NP films with different PEG4000 contents on the FTO substrate. For ease of presentation, we have recorded the NiO_x NP films with different PEG4000 contents as NiO_x-0, NiO_x-0.05, NiO_x-0.25 and NiO_x-0.50 films, where the numbers correspond to the weight ratio of PEG4000 to the NiO_x slurry, respectively. As shown in Fig. 3(a) and Fig. S3a (ESI†), even a small amount of added PEG4000 can effectively reduce the agglomeration of the particles and improve the

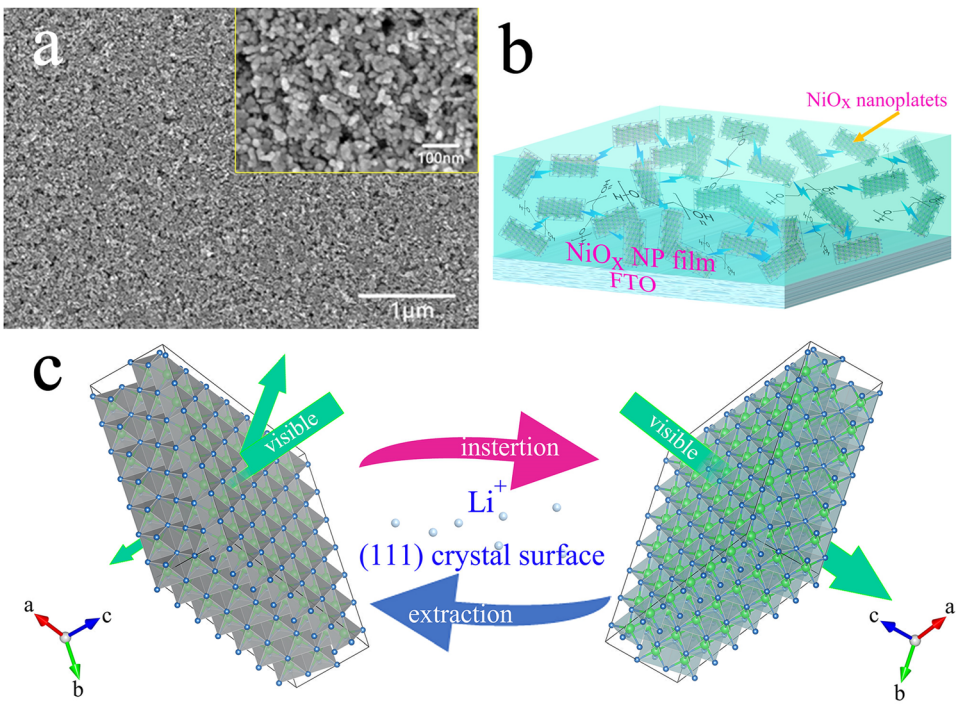

Fig. 3 (a) SEM images of NiO_x-0.05 films. (b) Schematic diagram of the structure of a NiO_x NP film. (c) Schematic representation of the electrochromic mechanism of lithium ion insertion/extraction NiO (111) surfaces.

uniformity of particle distribution. This can be attributed to the spatial dislocation effect and dispersing effect of PEG4000 which induces a certain repulsive force between nanoparticles,[45] increasing the uniformity of the nanoparticle coating and interconnecting NPs to form a porous nanoplatelet network-like structure (Fig. 3(b)). As is known from the TEM images above, the NiO nanoplatelets have in fact a certain orientation, so that the (111) surface exposed by the interconnected NPs becomes the preferential crystallographic surface for the insertion/extraction of the lithium ions during the electrochromic process. Fig. 3(c) shows the schematic correlation between the lithium ion insertion/extraction and the electrochromic process of the NiO_x NPs. As the PEG4000 content is increased, the pore structure of the films became more pronounced and unevenly distributed, forming a nickel oxide foam structure with uneven pore sizes, which is ascribed to the large amount of PEG4000 filling regions between the NiO_x NPs and then evaporating during the 300 °C annealing, thereby forming the irregular pores (Fig. S3b, ESI†). As the amount of PEG4000 is increased further, the pore structure of the films increases significantly and the distribution becomes even more inhomogeneous (Fig. S3c, ESI†). From the effect of the PEG4000 on the spatial morphology of the NP films, it can be inferred that involvement of PEG4000 may affect the kinetics of the ©on transport during the electrochromic process.

To investigate the electrochromic properties of the NiO_x NP film, UV-vis transmittance and electrochemical measurements of the films were carried out in 1M PC/$LiClO_4$ solution. Fig. 4(a) shows the transmittance spectra of different films in 1 M PC/$LiClO_4$ solution for the bleaching state (T_b) and the colouring state (T_c). It can be seen that involvement of PEG4000 affects obviously the T_b of the film which decreases monotonously with increasing PEG4000. On the other hand, T_c remains fairly unchanged for the three concentration of PEG4000, however, which is evidently lower than that of the film without PEG4000. The decrease in bleaching state transmission may be due to the presence of large non-uniform pores, which affect the flatness of the film, and the residual PEG4000 which hinders the discolouration of the NiO_x particles. The maximum contrast (ΔT) at 550 nm for the NiO_x-0, NiO_x-0.05, NiO_x-0.25 and NiO_x-0.50 films are 58.65, 63.09, 53.59 and 46.21%, respectively. It can be noticed that the NiO_x NPs exhibit a high optical contrast of 58.65 even without adding PEG4000, which is much higher than the NiO_x films synthesized by reported wet chemical methods and comparative to the one obtained by physical vapor deposition under high vacuum. To demonstrate the colour change of the films, we show the logo of our School of Materials Science & Engineering (MSE) under the bleached (−1.0 V) and coloured (1.7 V) states of the NiO_x-0.05 film (Fig. 4(b)), and the electrochromic process is also presented in Video S1 (the size of the film on display is 3 × 5 cm, while the size of the film used for testing is 0.6 × 5 cm). Excellent contrast of over 63.09% is achieved for the sample NiO_x-0.05. We tend to ascribe the high optical contrast to the uniform, fine and well-dispersed platelet-like NiO_x nanoparticle and well-defined Ni^{3+} vacancies as well. When NiO_x films are immersed into the PC/$LiClO_4$ electrolyte during anodic/cathodic scanning, the insertion/extraction of Li^+ ions in the host lattice causes charge transport between Ni^{2+}, Ni^{3+} and Ni^{4+}.[46] The process of intercalation/deintercalation of Li^+ ions in NiO_x films can be represented by:[46]

$$NiO_x + yLi + ye^- \rightleftharpoons Li_yNiO_x \quad (1)$$

$$Li_yNiO_x \rightleftharpoons Li_{y-z}NiO_x + zLi^+ + ze^- \quad (2)$$

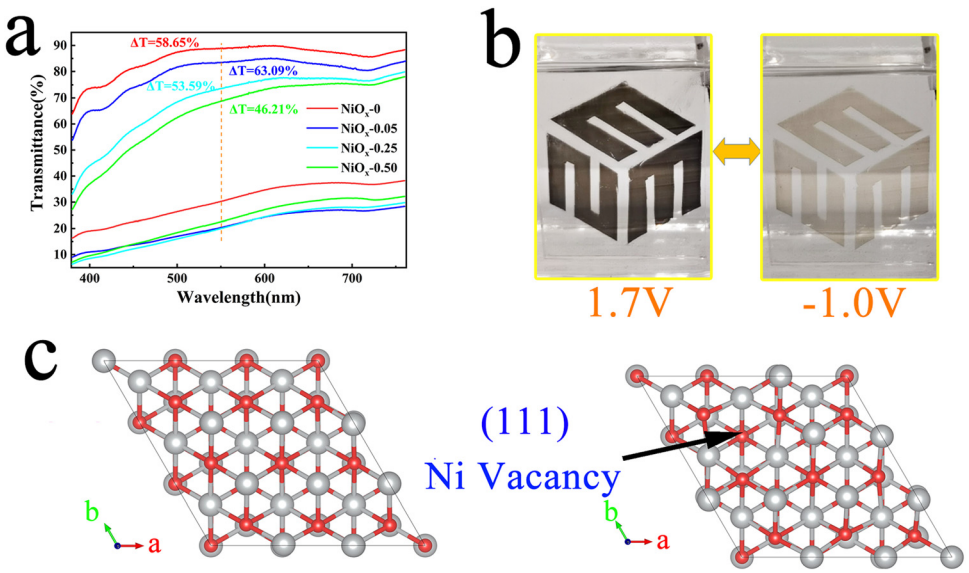

Fig. 4 Electrochemical and electrochromic properties of various NiO_x NP films in 1 M PC/$LiClO_4$ solution. (a) Transmission spectra of NiO_x NP films with different PEG4000 contents measured at −1.0 V and 1.7 V and 550 nm; (b) photographs of fully faded and fully coloured states of the NiO_x-0.05 film; (c) surface structures of NiO Ball-and-stick model of the surface of NiO: α (111) surface and β (111) surface with a Ni vacancy, where the red ball is an oxygen atom and the gray ball is a nickel atom.

When a negative voltage is applied, Li^+ ions are inserted, Ni^{3+} and Ni^{4+} are reduced to Ni^{2+} and the film changes from black to transparent; as shown in Fig. S1 (ESI†), when positive voltage is applied, the Li^+ ions are removed, Ni^{2+} are again oxidised to Ni^{3+} and Ni^{4+} and the film becomes black again. Non-stochiometric NiO_x has more nickel vacancies, which improves the EC performance of the film.[33] In terms of the formation mechanism of Ni vacancies, we attribute this to the lower vacancy formation energy of NiO making it susceptible to losing electrons during thermal movement and acquiring an oxygen ion from its surroundings, thus manifesting itself structurally as a Ni vacancy and macroscopically as an oxygen excess, with the mechanism diagram shown in Fig. S4 (ESI†). Due to the crucial influence of nickel vacancies on the EC properties of NiO_x, the formation of Ni vacancies on different crystal surfaces of NiO was investigated by theoretical simulation. The vacancy formation energy of the (111), (200) and (220) surfaces of NiO is calculated by using the first principle calculation method. In the calculation, we use a $3 \times 3 \times 3$ supercell with a 5-layer structure and a 20 Å vacuum layer to simulate the surface structure, in which the atoms of the lower 2 layers are fixed and the top three layers near the surface are relaxed, and the crystal surface structure is shown in Fig. 4(c) and Fig. S5 (ESI†). All calculations are implemented through the density functional theory (DFT) software package Vienna *Ab initio* Simulation Package (VASP). The projector augmented wave (PAW) potentials and the exchange-correlation functional of Perdew–Burke–Ernzerhof revised for solids (PBEsol) are used to emulate the ion cores and valence electrons. In the process of structure relaxation, we set the criterion of the force acting on each atom to be less than 10^{-2} eV $Å^{-1}$, and set the energy convergence criterion to 10^{-5} eV to fully optimize the supercell, a cutoff energy of 500 eV is used, where the *k*-point mesh is $5 \times 5 \times 1$ to sample the Brillouin zone. After the relaxation, we make a static calculation with high accuracy, the cutoff energy is 600 eV and energy convergence criterion is 10^{-7} eV.

The calculation formula of the formational energy of Ni vacancy is:

$$E_f = \frac{1}{S}(E_{sur} - E_{sur\text{-}Ni} - E_{Ni})$$

Here E_{sur} is the energy of the complete surface, $E_{sur\text{-}Ni}$ is the energy of the surface with a Ni atom vacancy, E_{Ni} is the energy of independent Ni atoms, and S is the surface area of the supercell. The results are shown in Table 1, from which we can see that it is easier to form a Ni vacancy on the surface of the (200) surface. But the (111) surface has a lower surface formation energy, so the probability of (111) faces in the material is higher, and there will be more total vacancies on the (111) faces. Considering the oriented growth of the NiO nanoplatelets along the (111) crystal planes, more Ni vacancies would participate in the electrochromic process which is the crucial reason why the NiO_x NP film in this work shows exceptional electrochromic performance.

In order to investigate whether the NiO_x NPs underwent any structural phase change during the slurry preparation and subsequent heat treatment, we measured the XRD patterns of the films with different PEG4000 contents. Fig. S6 (ESI†) shows that the NiO_x peaks are present in all samples, implying superior stability of the NPs even after the slurry preparation and annealing treatment.

Table 1 The formation energy of a Ni vacancy on different surfaces of NiO

Surface	S (Å^2)	E_{sur} (eV)	$E_{sur\text{-}Ni}$ (eV)	E_{Ni} (eV)	E_f (meV Å^{-2})
(111)	69.6175	−257.83991	−255.11612	1.52272	5.28×10^{-3}
(200)	69.6175	−257.19962	−255.60990	1.52272	4.37×10^{-3}
(220)	80.3874	−340.13064	−332.52972	1.52272	4.26×10^{-3}

On the other hand, FTIR was used to characterize the films after annealing at 300 °C to determine the surface functional groups in the films that may affect the EC performance. As shown in Fig. S6b (ESI†), the peak at around 1631 can be assigned to surface OH^- groups, the intensity of which is almost the same in NiO_x-0.05 and NiO_x-0 films, and becomes evidently higher in the NiO_x-0.25 film and keeps increasing in the NiO_x-0.5 film, which suggests more OH^- groups are generated with increasing PEG4000. According to TEM observation, the nanoparticles are mainly NiO_x nanoplatelets with exposed (111) facets which are inclined to absorb OH^- groups since the (111) planes of NiO terminate with nickel atoms. Therefore, excessive OH^- groups on the (111) facets of the NiO_x NPs would inevitably lower the EC performance. On the other hand, as the amount of PEG4000 added increases, the stronger the peaks at around 2930 and 2970 cm^{-1}, which can be attributed to the stretching vibration of the hydrocarbon bond (–CH) of the saturated carbon in PEG.[47] The intensity and width of the peaks for the NiO_x-0.50 film are significantly larger than those of the NiO_x-0.25 film, indicating a higher residual amount of PEG4000 in the former. In contrast, only very faint peaks are observed in the NiO_x-0.05 film. This indicates that more residue was generated after the annealing in the film with a greater PEG4000 amount.

Electrochromic switching speed is one of the main criteria for assessing the EC performance of a material, which reveals the electrochemical redox kinetics during the electrochromic process. The switching speed can be revealed by colouring/bleaching time, which is basically defined as the time taken to reach 90% of the optimum modulation. The results of *in situ* transmission measurements at 550 nm on different films in 1 M PC/$LiClO_4$ solution are shown in Fig. 5(a). The calculated colouring/bleaching times (t_c/t_b) for the NiO_x-0, NiO_x-0.05, NiO_x-0.25 and NiO_x-0.50 films are 2.0/2.0 s, 1.7/1.5 s, 2.1/2.0 s and 2.1/1.9 s, respectively. Of these, NiO_x-0.05 exhibits the fastest colouring and bleaching times. This is consistent with the SEM observation, and the homogeneous and high density pore structure of the NiO_x NP film was formed by adding an appropriate amount of PEG4000, which shortens the diffusion path of ions and increases the rate of ion diffusion during the colouring/bleaching process. On the other hand, the bonding and dispersing effect of PEG4000 may make the NPs well-connected to promote the electron transport which was investigated by electrochemical impedance spectroscopy. It is known

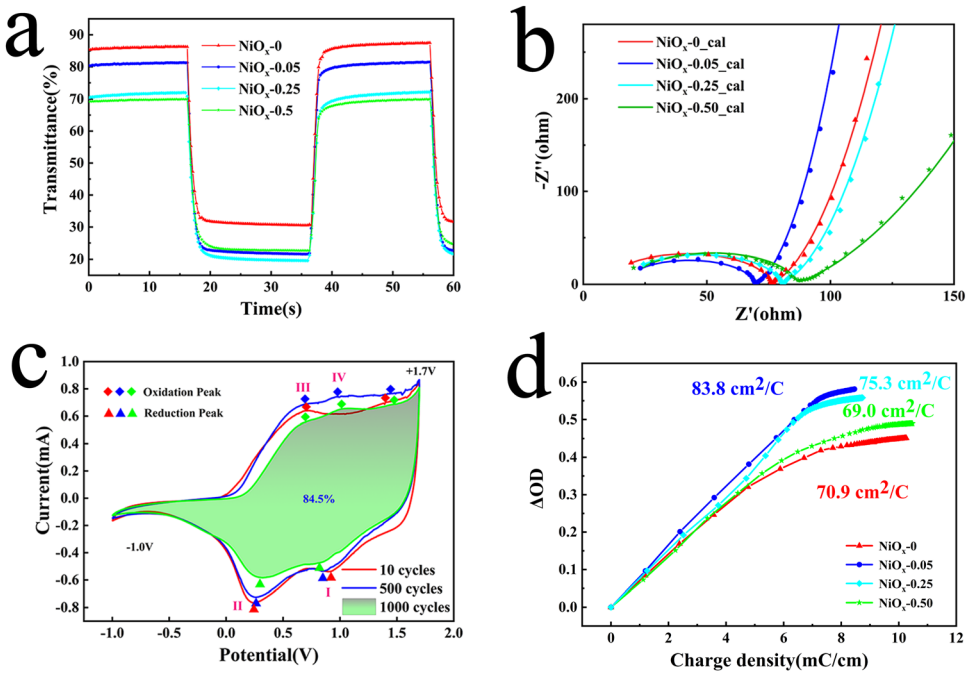

Fig. 5 Electrochemical and electrochromic properties of various NiO_x NP films in 1 M PC/$LiClO_4$ solution. (a) Dynamic transmittance spectra of the NiO_x NP films with different PEG4000 content at 550 nm. (b) Nyquist plots and corresponding simulation results (solid lines) of the different films in the initial state; (c) cyclic voltammetry curves of the NiO_x-0.05 film obtained at a scanning rate of 50 mV s^{-1} at the 10th, 500th and 1000th cycles; (d) colouring efficiency plots.

that electrochemical impedance spectroscopy (EIS) is a powerful technique used for the analysis of interfacial charge behaviours of electrochemical systems, which is used here to investigate the effect of PEG4000 on the charge transfer and mass transport in the NiO_x NP film. The Nyquist plots and corresponding fits for different films in 1 M PC/$LiClO_4$ solution are shown in Fig. 5(b). All samples show a semicircle in the high frequency region and a relatively straight line in the low frequency region. The semicircles indicate the charge transfer impedance at the electrode/electrolyte interface, while the slope of the lines are attributed to the diffusion of Li^+ in the material. In general, the smaller the semicircle the lower the corresponding impedance, while the higher slope of the line indicates a faster ion diffusion rate.[48] The equivalent circuit diagram used to evaluate the electrochemical impedance spectroscopy spectrum of the thin films is shown in the inset in Fig. 5(b), where R_e is the electrolyte resistance, R_{ct} is the charge transfer resistance, C_{dl} is the relevant constant phase element, Z_w represents the Warburg impedance associated with ion diffusion, and C_l represents the low frequency mass capacitance.[49] Based on the equivalent circuit diagram, the total resistances (R_t) of the NiO_x-0, NiO_x-0.05, NiO_x-0.25 and NiO_x-0.50 films can be calculated to be 12.69, 10.35, 15.88 and 18.53 Ω, respectively. Table S1 (ESI†) summarises the extracted values of the various resistance and capacitance values for the films. The measurement indicates that a small amount of PEG4000 can speed up the electronic injection in the electrode and simultaneous ionic insertion from solution, thereby promoting the switching speed.

As a persistent endeavour, it is attractive but challenging to obtain electrochromic nickel oxide films with high cycling stability. Cyclic voltammetry (CV) curves and the corresponding transmittance spectra of the NiO_x-0.05 film were measured at the 10th, 500th and 1000th cycles as shown in Fig. 5(c) and Fig. S6 (ESI†), which also indicates the reaction pathways. The CV curves can be divided into two parts: the cathodic reaction curve (bleaching process in reduction) and anodic reaction curve (colouring process in oxidation). In the cathodic reaction curve, the two broad peaks can be ascribed to the reduction of Ni^{4+} (peak I) and Ni^{3+} (peak II) due to the deintercalation of lithium ions. In terms of the anodic reaction curve, two oxidation peaks of nickel ions (peak III and peak IV) can be discerned, while the peak IV is absent in the 10th cycle curve and is present in the 500th cycle curve, suggesting an activation process in the colouring/bleaching process. Likewise, calculation results suggest that the area of the CV curve at the 500th cycle is larger than that at the 10th cycle (Fig. 5(c)), which can be attributed to the increase in film ion storage during the long-term activation phases of the cycling phase.[50] Correspondingly, the maximum contrast of the NiO_x-0.05 film at 550 nm is increased from 63.09 to 64.23% (Fig. S7, ESI†). After the 1000th cycle, the maximum contrast of the film still keeps 95% of the initial value suggesting slow property degradation. In addition, the CV curves demonstrate stable reduction and oxidation of nickel ions accompanying the intercalation/deintercalation of lithium ions during the cycling process, which is one reason why the NiO_x NP films exhibit superior durability. On the other hand, PEG4000 was found to have another important role in determining the cycling stability of the NiO_x NP films. The changes in CE and switching speed of NiO_x-0.05 films were also evaluated during cycling and it was found that the film still kept a high CE value after

1000 cycles, while the dynamic transmittance spectra indicated that the film remained highly reversible after cycling (Fig. S8, ESI†). Fig. S9 (ESI†) shows the cycling stability of the NP films with different amounts of PEG4000. While the optical contrast of the NiO_x-0 and NiO_x-0.50 films shows a significant drop after 250 cycles, that of the NiO_x-0.05 film remains almost constant even after 1000 cycles. This is due to the homogeneous porous structure of the NiO_x-0.05 film which provides an effective buffer to volume change and more ion binding sites, while the small amount of residual PEG4000 acts as a binder between the NiO_x NPs, which in turn results in a more robust structure and greater ion transport. However, excess PEG4000 changes the structure/morphology of the resulting in substantially reduced contact area between the film and the substrate, making the film more likely to detach from the substrate during the cycling test.

From the view of the energy utilization efficiency in an electrochromic process, colouring efficiency is an important figure of merit showing the dependence of optical density (ΔOD) on the unit charge density (Q/A), with higher CE values representing the ability of the material to bring about a larger change in transmittance through a smaller amount of charge. The CE value can be obtained using the following equation:[51]

$$\mathrm{CE} = \frac{\Delta \mathrm{OD}}{Q/A} = \frac{\log(T_b/T_c)}{Q/A} \quad (3)$$

Where T_b and T_c are the transmittance of the film in the bleached and coloured states, respectively, A is the effective working area and Q is the charge. Fig. 5(d) shows the colouring efficiency (CE) plots for NiO_x-0, NiO_x-0.05 and NiO_x-0.50 films, respectively. It can be seen that the NiO_x-0.05 film has higher CE than the other films with a CE of 83.8 $cm^2\ C^{-1}$ (−1.0 to 1.7 V). In contrast the NiO_x-0 film without PEG4000 shows a lower CE of only 70.9 $cm^2\ C^{-1}$. On the other hand, excess addition of PEG4000 also impedes the CE in which the NiO_x-0.25 and NiO_x-0.50 films show CEs of 75.3 and 69.0 $cm^2\ C^{-1}$, respectively. In order to compare the performance of different films, Table S2 (ESI†) summarizes the electrochromic properties of the films.

At the same time, to demonstrate the importance of Ni vacancies, Ar-NiO_x NPs with fewer Ni vacancies were prepared under an Ar atmosphere. The weaker resonant EPR signals indicate their reduced concentration of Ni vacancies (Fig. S10, ESI†). Thus, when the films were prepared and tested for performance using the same parameters, the AR-NiO_x films exhibited poorer performance (ΔT decreased to 55.9% and their switching speed slowed of 2.2 s/1.6 s), indicating that the presence of Ni vacancies effectively enhanced the performance of the films (Fig. S11a and b, ESI†). In conclusion, the excellent performance can be attributed to the nanosized structure providing more ion binding sites and shortening the ion/electron transport distance, while the NiO_x nanoplates structure with a certain orientation has a positive effect on the current modulation of the film[26] and the presence of Ni vacancies bestows NiO_x with a better hole conductivity. Since the ionic insertion/extraction during the electrochromic process also produces pseudo-capacitive behaviour, the high CE of the NP film signifies its potential in energy storage applications.

Therefore, capacitive characteristics of the NPs was investigated. Fig. 6(a) shows the galvanostatic charge–discharge (GCD)

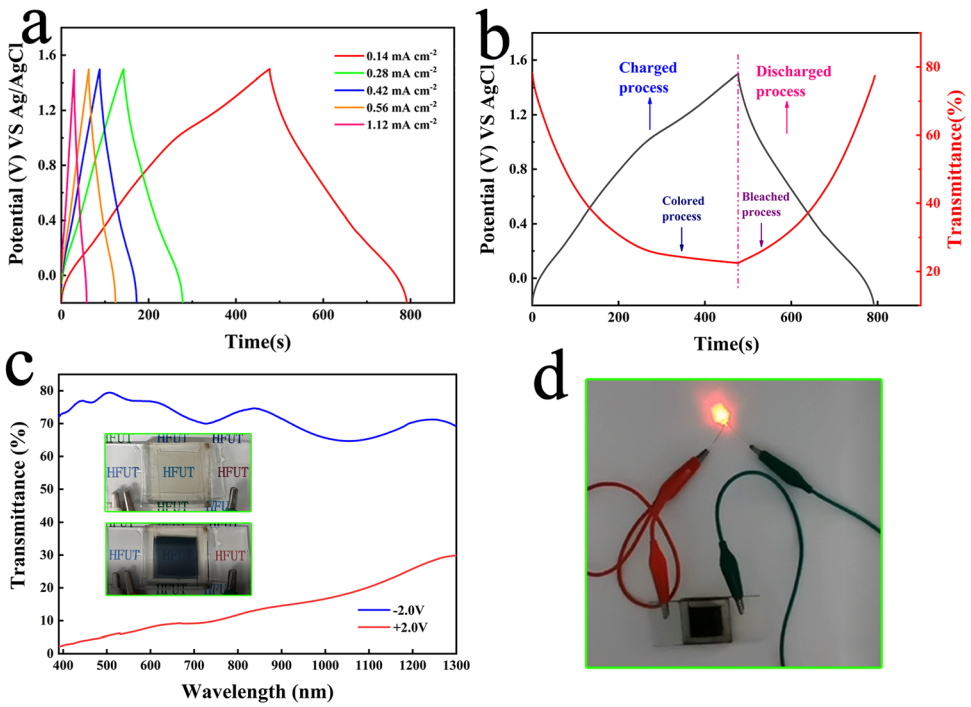

Fig. 6 NiO_x-0.05 NP films: (a) galvanostatic charge/discharge curves at different current densities and (b) galvanostatic charge/discharge curves at 0.14 mA cm^{-2} in the voltage range of −0.3 to 1.7 V and the corresponding dynamic optical response at 550 nm; (c) transmission spectra of ECDs; (d) image of lit up small LED bulbs.

Table 2 Comparison of the EC performance of various reported NiO films in 1 M PC/$LiClO_4$ solutions

Films	Preparation method	ΔT (%)	t_b (s)	t_c (s)	CE $cm^2\ C^{-1}$ (λ/nm)	Ref.
NiO	RF magnetron sputtering	34	np	np	30(550)	53
NiO_x	DC magnetron sputtering	62	17	9.8	62(550)	34
Sn–NiO	RF magnetron sputtering	65.1	1.4	1.3	39.3(660)	54
NiO	RF magnetron sputtering	55	4.1	9.9	24.4(550)	35
NiO_x	RF magnetron sputtering	40	np	np	67(550)	55
NiO	E-beam evaporation	66(0.5M PC/Li^+)	1.4	3.6	55(630)	56
Inverse opal NiO	Electrodeposition	16.2	np	np	np	57
NiO/V_2O_5	CBD+ Electrodeposition	35	11	8	30.6(776)	58
NiO	Combustion reaction	34	2.3	16.9	92.3(550)	59
NiO_x	Scrape-coating	63.1	1.5	1.7	83.8(550)	This work

curves of NiO_x NP films collected at different current densities. In all cases, somewhat symmetrical GCD curves are obtained, demonstrating good reversibility of the sample. The calculated surface capacitance at different current density conditions is shown in Fig. S12 (ESI†). When the current density is 0.14 mA cm^{-2}, the surface capacitance can reach up to 26.07 mF cm^{-2}, and when the current density increases to 1.12 mA cm^{-2}, the surface capacitance can be kept at 73% of the highest value, which indicates that the film has a good multiplicative performance. Fig. 6(b) shows the variation of *in situ* transmittance of the film at 550 nm and the GCD curve in the voltage range of −0.3 to 1.5 V and under 0.14 mA cm^{-2} charge/discharge conditions. The colour of the film changes to black-brown when fully charged at 1.5 V. The film turns back to the transparent state when it enters the discharge process at −0.3 V. Its excellent optical properties and good capacitive performance demonstrate its application in ECDs, therefore, NiO_x-WO_3 ECDs were prepared to demonstrate its electrochromic/energy storage dual function properties, where WO_3 was prepared by a simple sol–gel spin-coating method (detailed information is shown in S13 and Fig. S13, ESI†). As shown in Fig. 6(c), the ECDs exhibit a transmittance change of over 70%, with the image of the coloured state (+2 V) and bleached state (−2 V) shown in the inset in Fig. 6(c). Video.2 shows a movie of the electrochromic process of ECDs, showing how quickly ECDs can be converted in the coloured and bleached state. To demonstrate its energy storage properties, we connected small LED bulbs to the ends of the ECD in its fully coloured state and found that the bulbs were successfully lit by the ECD (Fig. 6(d)). However, ECDs cannot be operated at voltages above 3.5 V for long periods of time, as this will cause the NiO_x electrodes to fall off. This result suggests the high electrochromic-energy storage bifunctional performance of the NiO_x NPs in a lithium ion electrolyte environment, which still remains an immature research field.[52]

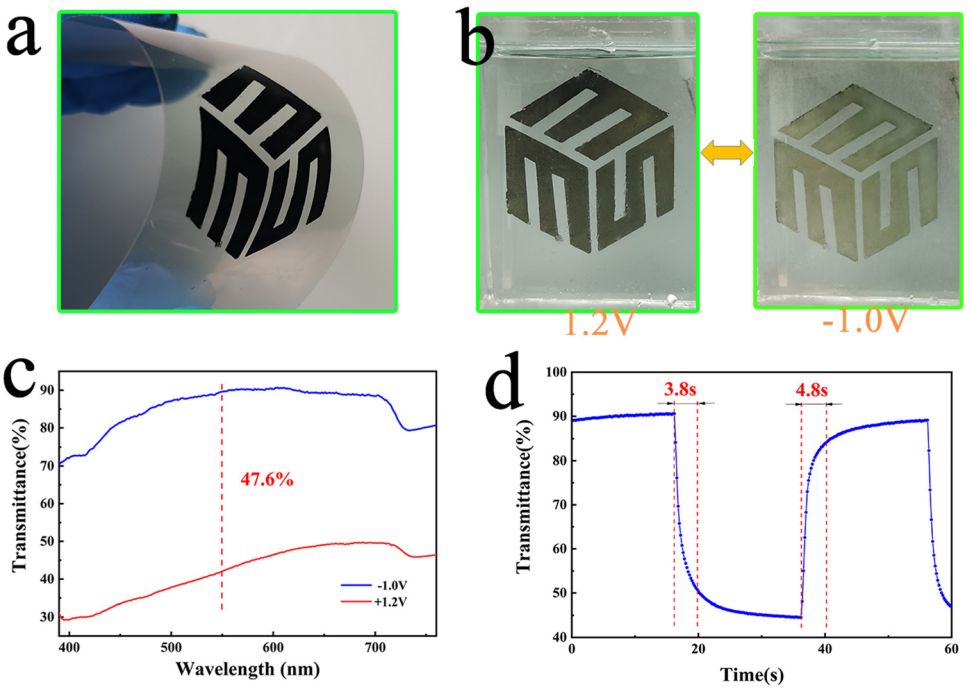

Fig. 7 (a) Photograph of the flexible NiO_x NP film; (b) photographs showing the fully faded and fully coloured states of the flexible NiO_x NP film; (c) transmittance spectra of the flexible NiO_x NP films measured at −1.0 V and 1.2 V at 550 nm. (d) Dynamic transmittance spectrum of the flexible NiO_x NP film at 550 nm showing the switching speed.

Physical vapour deposition (PVD) has been the main method to prepare NiO_x films that can change colour in PC/$LiClO_4$ electrolytes, but dense films which are prepared by magnetron sputtering and other methods make ion transport more difficult. Films prepared by wet chemical methods, on the other hand, have limited EC performance in PC/$LiClO_4$ because the NiO_x obtained is in the normal stoichiometric ratio and has some groups on the surface due to the thermal decomposition of the nickel oxide precursor. In Table 2, we compare the performance of our NiO_x NP films with those reported in the literature measured in PC/$LiClO_4$ solution, including those prepared by magnetron sputtering,[53–55] e-beam evaporation,[56] electrodeposition,[57] chemical bath deposition[58] and combustion reactions.[59] It can be seen that our NiO_x films have a significant improvement over most of the NiO_x films prepared by other methods, highlighting the superiority of this work and the potential for commercialisation.

To evaluate the possibility of the NiO_x NP film in flexible wearable devices and displays, we coated NiO_x-0 slurry on PEN-ITO conductive films and annealed them at low temperature (150 °C for 40 min), as shown in Fig. 7(a) and (b) shows the photos of fully faded and fully coloured states of the film in 1 M PC/$LiClO_4$ solution. It can be observed that the film shows a yellowish translucent state at −1 V, and changes to black when the voltage is increased to 1.2 V. Fig. 7(c) shows the film has a transmittance contrast of 47.6% at 550 nm whilst Fig. 7(d) shows a colouring time of 3.8 s and a bleaching time of 4.8 s, which is outstanding among the reported flexible NiO_x electrochromic layer.[60] Moreover, the flexible NiO_x NP films can undergo large angle (90°) bending for 400 times without property degradation, which exhibits superior mechanical flexibility owing to the precise addition of PEG4000 presenting a bonding effect. Nevertheless, further and detailed investigation is necessary to unveil the origin of the electrochromic performance and energy storage enhancement of the obtained NiO_x NP films and explore its potential in developing high performance flexible electrochromic-energy storage bifunctional devices.

Conclusions

In conclusion, NiO_x NP films were prepared using a facile and well-controlled scrape-coating technique chemical precipitation method which exhibited excellent electrochromic-energy storage bifunctional performance and stability in 1M PC/$LiClO_4$ solution. While the oriented crystal plane and nickel vacancies are essential in determining the EC performance of the NPs, the PEG4000 additive plays a crucial role in property enhancement. High transmittance modulation (63.09%), fast switching speed (colouring time 1.7 s/bleaching time 1.5 s), high CE value (up to 83.8 $cm^2\ C^{-1}$) and high stability (about 95% after 1000 cycles) of the NP film were obtained by adjusting the PEG4000 addition, which exhibited superior lithium ion storage capability as well. At the same time, the higher CE values (45.12 $cm^2\ C^{-1}$) and reversibility are retained after the cycle. These characteristics can be attributed to the dispersion effect of PEG4000 in reducing agglomeration and adding some porosity to the film. Furthermore, ECDs based on NiO_x nanoplatelet films and WO_3 films exhibit excellent electrochromic/energy storage properties. Furthermore, flexible NiO_x NP films on the PEN-ITO substate were also achieved which showed high transmittance modulation (47.6%) and good mechanical flexibility. The strategy in this work proposes an alternative and promising way for developing high performance flexible electrochromic-energy storage bi-functional materials and devices with the advantages of vacuum-free, large area and cost effectiveness.

Author contributions

Xinyu Tao: writing-original draft, writing-reviewing and editing, methodology, and investigation; Yong Zhang: resources, methodology, investigation, supervision, project administration, and writing-reviewing and editing; Jingyi Cai: methodology and investigation; Hark Hoe Tan: writing-reviewing and software; Jiewu Cui: validation and investigation; Yan Wang: validation and software; Xia Shu: methodology and investigation; Zhenhong Dai: first principles calculation, and software; Yongqiang Qin: investigation; Jiaqin Liu: investigation and supervision; Yucheng Wu: resources, project administration, and editing.

Conflicts of interest

There are no conflicts to declare.

Acknowledgements

This project is supported by the National Natural Science Foundation of China (Grant No. 52072106, U1810204, 52172293, 51972093), the Key R&D Projects of Anhui Province (202104b11020016), the Natural Science Foundation of Anhui Province (2108085MB45), and the Fundamental Research Funds for the Central Universities (PA2021KCPY0044, PA2021GDSK0088, PA2021GDSK0094). We would also like to acknowledge the financial support from the Higher Education Discipline Innovation Project ''New Materials and Technology for Clean Energy'' (B18018) H. H. T. acknowledges the award of the Overseas Distinguished Professorship (Haiwai Mingshi) by the Chinese Ministry of Education.

References

1 P. H. Yang, P. Sun and W. J. Mai, Electrochromic energy storage devices, *Mater. Today*, 2016, **19**, 394–402.
2 Q. R. Liu, Q. Q. Chen, Q. Q. Zhang, G. B. Dong, X. L. Zhong, Y. Xiao, M. Delplancke-Ogletree, F. Reniers and X. G. Diao, Dynamic behaviors of inorganic all solid state electrochromic device: Role of potential, *Electrochim. Acta*, 2018, **269**, 617–623.
3 T. G. Yun, M. Park, D. H. Kim, J. Y. Cheong, J. G. Bae, S. M. Han and I. D. Kim, All transparent-stretchable

electrochromic-supercapacitor wearable patch device, *ACS Nano*, 2019, **13**, 3141–3150.

4 J. W. Xie, J. M. Zhang, Y. Y. Ma, Y. H. Han, J. F. Li and M. Zhu., Spiropyran-incorporated honeycomb porous films with reversible multistimuli-responsive properties, *J. Mater. Chem. C*, 2022, **10**, 7154–7166.

5 G. F. Cai, J. X. Wang and P. S. Lee, Next-generation multifunctional electrochromic devices, *Acc. Chem. Res.*, 2016, **49**, 1469–1476.

6 T. Xu, E. C. Walter, A. Agrawal, C. Bohn, J. Velmurugan, W. Q. Zhu, H. J. Lezec and A. A. Talin, High-contrast and fast electrochromic switching enabled by plasmonics, *Nat. Commun.*, 2016, **7**, 10479.

7 X. T. Huo, R. Li, J. K. Wang, M. Zhang and M. Guo, Repairable electrochromic energy storage devices: A durable material with balanced performance based on titanium dioxide/tungsten trioxide nanorod array composite structure, *Chem. Eng. J.*, 2022, **430**, 132821.

8 S. Y. Kim, Y. J. Jang, Y. M. Kim, J. K. Lee and H. C. Moon, Tailoring diffusion dynamics in energy storage ionic conductors for high-performance, multi-function, single-layer electrochromic supercapacitors, *Adv. Funct. Mater.*, 2022, **32**, 2200757.

9 Y. J. Jang, S. Y. Kim, Y. M. Kim, J. K. Lee and H. C. Moon, Unveiling the diffusion-controlled operation mechanism of all-in-one type electrochromic supercapacitors: Overcoming slow dynamic response with ternary gel electrolytes, *Energy Storage Mater.*, 2021, **43**, 20–29.

10 S. Y. Kim, T. Y. Yun, K. S. Yu and H. C. Moo, Reliable, high-performance electrochromic supercapacitors based on metal-doped nickel oxide, *ACS Appl. Mater. Interfaces*, 2020, **12**, 51978–51986.

11 I. B. Pehlivan, G. Atak, G. A. Niklasson, L. Stolt, M. Edoff and T. Edvinsson, Electrochromic solar water splitting using a cathodic WO_3 electrocatalyst, *Nano Energy*, 2021, **81**, 105620.

12 Y. D. Shi, M. J. Sun, Y. Zhang, J. W. Cui, X. Shu, Y. Wang, Y. Q. Qin, J. Q. Liu, H. H. Tan and Y. C. Wu, Rational design of oxygen deficiency-controlled tungsten oxide electrochromic films with an exceptional memory effect, *ACS Appl. Mater. Interfaces*, 2020, **12**, 32658–32665.

13 S. X. Song, Y. Liu, X. J. Liu, J. P. Ge, D. T. Ge and L. L. Yang, Color brightness modulation of a responsive photonic liquid for multicolored electrochromic displays, *J. Mater. Chem. C*, 2022, **10**, 3114–3120.

14 P. J. Wojcik, A. S. Cruz, L. Santos, L. Pereira, R. Martins and E. Fortunato, Microstructure control of dual-phase inkjet-printed a-WO_3/TiO_2/WO_X films for high-performance electrochromic applications, *J. Mater. Chem.*, 2012, **22**, 13268–13278.

15 J. H. Zhang, G. F. Cai, D. Zhou, H. Tang, X. L. Wang, C. D. Gu and J. P. Tu, Co-doped NiO nanoflake array films with enhanced electrochromic properties, *J. Mater. Chem. C*, 2014, **2**, 7013–7021.

16 J. Y. Xue, H. B. Xu, S. Wang, T. T. Hao, Y. Yang, X. Zhang, Y. Song, Y. Li and J. P. Zhao, Design and synthesis of 2D rGO/NiO heterostructure composites for high-performance electrochromic energy storage, *Appl. Surf. Sci.*, 2021, **565**, 150512.

17 G. F. Cai, J. P. Tu, J. Zhang, Y. J. Mai, Y. Lu, C. D. Gu and X. L. Wang, An efficient route to a porous NiO/reduced graphene oxide hybrid film with highly improved electrochromic properties, *Nanoscale*, 2012, **4**, 5724–5730.

18 L. L. Xiao, Y. Lv, W. J. Dong, N. Zhang and X. Y. Liu, Dual-functional WO_3 nanocolumns with broadband antireflective and high-performance flexible electrochromic properties, *ACS Appl. Mater. Interfaces*, 2016, **8**, 27107–27114.

19 S. Hou, X. Zhang, Y. L. Tian, J. P. Zhao, H. B. Geng, H. Y. Qu, H. C. Zhang, K. Zhang, B. S. Wang, A. Gavrilyuk and Y. Li, Improved electrochemical cycling durability in a nickel oxide double layer film, *Chem. – Asian J.*, 2017, **12**, 2922–2928.

20 K. K. Chiang and J. J. Wu, Fuel-assisted solution route to nanostructured nickel oxide films for electrochromic device application, *ACS Appl. Mater. Interfaces*, 2013, **5**, 6502–6507.

21 J. H. Zhang, J. P. Tu, D. Zhou, H. Tang, L. Li, X. L. Wang and C. D. Gu, Hierarchical SnO_2@NiO core/shell nanoflake arrays as energy-saving electrochromic materials, *J. Mater. Chem. C*, 2014, **2**, 10409–10417.

22 J. H. Yu, S. H. Nam, Y. E. Gil and J. H. Boo, The effect of ammonia concentration on the microstructure and electrochemical properties of NiO nanoflakes array prepared by chemical bath deposition, *Appl. Surf. Sci.*, 2020, **532**, 147441.

23 K. Chen, Y. K. Wu, L. Y. You, W. T. Wu, X. K. Wang, D. Zhang, J. F. Elman, M. Ahmed, H. Wang, K. J. Zhao and J. G. Mei, Printing dynamic color palettes and layered textures through modeling-guided stacking of electrochromic polymers, *Mater. Horiz.*, 2022, **9**, 425–432.

24 M. Rakibuddin, M. A. Shinde and H. Kim, Sol–gel fabrication of NiO and NiO/WO_3 based electrochromic device on ITO and flexible substrate, *Ceram. Int.*, 2020, **46**, 8631–8639.

25 K. H. Wang, H. Ikeuchi, M. Yoshida, T. Miura, I. P. Liu, G. Watanabe, S. Y. Cui and T. Kawai, Nanometer-thick nickel oxide films prepared from alanine-chelated coordination complexes for electrochromic smart windows, *ACS Appl. Nano Mater.*, 2020, **3**, 9528–9537.

26 S. Nandy, G. Gonçalves, J. V. Pinto, T. Busani, V. Figueiredo, L. Pereira, R. F. P. Martins and E. Fortunato, Current transport mechanism at metal–semiconductor nanoscale interfaces based on ultrahigh density arrays of p-type NiO nano-pillars, *Nanoscale*, 2013, **5**, 11699–11709.

27 P. Grey, L. Pereira, S. Pereira, P. Barquinha, I. Cunha, R. Martins and E. Fortunato, Solid state electrochemical WO3 transistors with high current modulation, *Adv. Electron. Mater.*, 2016, **2**, 1500414.

28 M. Y. Wang, Y. C. He, M. D. Rocha, A. Rougier and X. G. Diao, Temperature dependence of the electrochromic properties of complementary NiO‖WO_3 based devices, *Sol. Energy Mater. Sol. Cells*, 2021, **230**, 111239.

29 P. Pooyodying, J. W. Ok, Y.-H. Son and Y. M. Sung, Electrical and optical properties of electrochromic device with WO_3: Mo film prepared by RF magnetron Co-Sputtering, *Opt. Mater.*, 2021, **112**, 110766.

30 S. J. Lee, T. G. Lee, S. Nahm, D. H. Kim, D. J. Yang and S. H. Han, Investigation of all-solid-state electrochromic devices with durability enhanced tungsten-doped nickel oxide as a counter electrode, *J. Alloys Compd.*, 2020, **815**, 152399.

31 J. H. Qiu, Z. Chen, T. X. Zhao, Z. H. Chen, W. J. Chu, N. Y. Yuan and J. N. Ding, Electrochromic properties of NiO_x films deposited by DC magnetron sputtering, *J. Nanosci. Nanotechnol.*, 2018, **18**, 4222–4229.

32 J. R. A. Acuña, I. Perez, V. Sosa, F. Gamboa, J. T. Elizalde, R. Farías, D. Carrillo, J. L. Enríquez, A. Burrola and P. Mani, Sputtering power effects on the electrochromic properties of NiO films, *Optik*, 2021, **10**, 166509.

33 J. J. Guo, M. Wang, Z. B. Zhang, G. B. Dong, F. M. Liu, H. Wang, H. Yu, Y. Xiao, J. Liu and X. G. Diao, Vacancy dependent electrochromic behaviors of NiO_x anodes: As a single layer and in devices, *Sol. Energy Mater. Sol. Cells*, 2018, **178**, 193–199.

34 D. M. Dong, W. W. Wang, G. B. Dong, F. Zhang, Y. C. He, H. Yu, F. M. Liu, M. Wang and X. G. Diao, Electrochromic properties and performance of NiO_x films and their corresponding all-thin-film flexible devices preparedby reactive DC magnetron sputtering, *Appl. Surf. Sci.*, 2016, **383**, 49–56.

35 G. H. Gao, S. Q. Xue, H. R. Wang, Z. H. Zhang, G. M. Wu, T. T. Debela and H. S. Kang, Highly thermally stable and transparent WO_3–SiO_2 gasochromic films obtained by an automated printing method, *ACS Sustainable Chem. Eng.*, 2021, **9**, 17319–17329.

36 S. D. Liu, L. Kang and S. C. Jun, Challenges and strategies toward cathode materials for rechargeable potassium-ion batteries, *Adv. Mater.*, 2021, **33**, 2004689.

37 L. Kang, M. Y. Zhang, J. Zhang, S. D. Liu, N. Zhang, W. J. Yao, Y. Ye, C. Luo, Z. W. Gong, C. L. Wang, X. F. Zhou, X. Wu and S. C. Jun, Correction: Dual-defect surface engineering of bimetallic sulfide nanotubes towards flexible asymmetric solid-state supercapacitors, *J. Mater. Chem. C*, 2020, **8**, 25443–25444.

38 S. D. Liu, L. Kang, J. Zhang, S. C. Jun and Y. Yamauchi, Carbonaceous anode materials for non-aqueous sodium- and potassium-ion hybrid capacitors, *ACS Energy Lett.*, 2021, **6**(11), 4127–4154.

39 S. D. Liu, L. Kang, J. Zhang, E. Jung, S. C. Lee and S. C. Jun, Structural engineering and surface modification of MOF-derived cobalt-based hybrid nanosheets for flexible solid-state supercapacitors, *Energy Storage Mater.*, 2020, **32**, 167–177.

40 F. Jiang, W. C. H. Choy, X. C. Li, D. Zhang and J. Q. Cheng, Post-treatment-free solution-processed non-stoichiometric NiO_x nanoparticles for efficient hole-transport layers of organic optoelectronic devices, *Adv. Mater.*, 2015, **27**, 2930–2937.

41 G. F. Cai, X. Wang, M. Q. Cui, P. Darmawan, J. X. Wang, A. L.-S. Eh and P. S. Lee, Electrochromo-supercapacitor based on direct growth of NiO nanoparticles, *Nano Energy*, 2015, **12**, 258–267.

42 N. M. Vuong, N. M. Hieu, D. Kim, B. I. Choi and M. Kim, Ni_2O_3 decoration of In_2O_3 nanostructures for catalytically enhanced methane sensing, *Appl. Surf. Sci.*, 2014, **317**, 765–770.

43 S. Y. Zhou, S. Wang, S. J. Zhou, H. B. Xu, J. P. Zhao, J. Wang and Y. Li, Electrochromic-supercapacitor based on MOF derived hierarchical-porous NiO film, *Nanoscale*, 2020, **12**, 8934–8941.

44 Y. L. Chen, Y. Wang, P. Sun, P. H. Yang, L. H. Du and W. J. Mai, Nickel oxide nanoflake-based bifunctional glass electrodes with superior cyclic stability for energy storage and electrochromic applications, *J. Mater. Chem. A*, 2015, **3**, 20614–20618.

45 Z. Q. Yuan, W. C. Tao, Z. D. Wang and W. M. Yang, One-step synthesis of highly dispersed nanosheets of magadiite, *Appl. Clay Sci.*, 2019, **181**, 105231.

46 Q. R. Liu, Q. Q. Chen, Q. Q. Zhang, Y. Xiao, X. L. Zhong, G. B. Dong, M. Delplancke-Ogletree, H. Terryn, K. Baert, F. Reniers and X. G. Diao, *In situ* electrochromic efficiency of a nickel oxide thin film: Origin of electrochemical process and electrochromic degradation, *J. Mater. Chem. C*, 2018, **6**, 646–653.

47 P. Koilraj, M. Takemoto, Y. Tokudome, A. Bousquet, V. Prevot and C. Mousty, Electrochromic thin films based on NiAl layered double hydroxide nanoclusters for smart windows and low-power displays, *ACS Appl. Nano Mater.*, 2020, **3**, 6552–6562.

48 Y. X. Wei, W. M. Liu, J. Y. Li, Z. Y. Fu and Y. Yan, Investigation on the properties of Li doped Ni–W oxide film and application for black electrochromic device, *Chem. Eng. J.*, 2022, **406**, 139833.

49 H. Liang, R. Li, C. Li, C. Y. Hou, Y. G. Li, Q. H. Zhang and H. Z. Wang, Regulation of carbon content in MOF-derived hierarchical-porous NiO@C films for high-performance electrochromism, *Mater. Horiz.*, 2019, **6**, 571–579.

50 I. Bouessay, A. Rougier, P. Poizot, J. Moscovici, A. Michalowicz and J.-M. Tarascon, Electrochromic degradation in nickel oxide thin film: A self-discharge and dissolution phenomenon, *Electrochim. Acta*, 2005, **50**, 3737–3745.

51 T. T. Hao, S. Wang, H. B. Xu, X. Zhang, J. Y. Xue, S. K. Liu, Y. Song, Y. Li and J. P. Zhao., Stretchable electrochromic devices based on embedded WO_3@AgNW Core-Shell nanowire elastic conductors., *Chem. Eng. J.*, 2021, **426**, 13084.

52 J. K. Wang, X. T. Huo, M. Guo and M. Zhang, A review of NiO-based electrochromic-energy storage bifunctional material and integrated device, *J. Energy Storage*, 2022, **47**, 103597.

53 G. Atak and Ö. D. Coşkun, Annealing effects of NiO thin films for all-solid-state electrochromic devices, *Solid State Ionics*, 2017, **305**, 43–51.

54 Y. M. Zhao, X. Zhang, X. Chen, W. J. Li, L. B. Wang, Z. T. Li, J. P. Zhao, F. Endres and Y. Li, Preparation of Sn–NiO films and all-solid-state devices with enhanced electrochromic properties by magnetron sputtering method, *Electrochim. Acta*, 2020, **367**, 137457.

55 Y. S. Lin, P.-W. Chen, D.-J. Lin, P.-Y. Chuang, T.-H. Tsai, Y.-C. Shiah and Y. C. Yu, Electrochromic performance of reactive plasma-sputtered NiO_x thin films on flexible PET/

ITO substrates for flexible electrochromic devices, *Surf. Coat. Technol.*, 2020, **205**, S216–S221.

56 S. Pereira, A. Gonçalves, N. Correia, J. Pinto, L. Pereira, R. Martins and E. Fortunato, Electrochromic behaviour of NiO thin films deposited by e-beam evaporation at room temperature, *Sol. Energy Mater. Sol. Cells*, 2014, **120**, 109–115.

57 H. Y. Qu, J. X. Wang, J. Montero, Y. Li, L. Österlund and G. A. Niklasson, Multicolored absorbing nickel oxide films based on anodic electrochromism and structural coloration, *J. Appl. Phys.*, 2021, **129**, 123105.

58 Y. N. Liu, C. Y. Jia, Z. Q. Wan, X. L. Weng, J. L. Xie and L. J. Deng, Electrochemical and electrochromic properties of novel nanoporous NiO/V_2O_5 hybrid film, *Sol. Energy Mater. Sol. Cells*, 2015, **132**, 467–475.

59 C. Lupo, F. Eberheim and D. Schlettwein, Facile low-temperature synthesis of nickel oxide by an internal combustion reaction for applications in electrochromic devices, *J. Mater. Sci.*, 2020, **55**, 14401–14414.

60 W. Z. Li, T. Bai, G. X. Fu, Q. Q. Zhang, J. B. Liu, H. Wang, Y. Y. Sun and H. Yan, Progress and challenges in flexible electrochromic devices, *Sol. Energy Mater. Sol. Cells*, 2022, **240**, 111709.